RESEARCH ARTICLE | SEPTEMBER 19 2025

Charge transport and electric field-dependent exciton dissociation in organic semiconductors measured using accumulation at an insulator–semiconductor layer

Asad Mahmood ; Mile Gao ; Mitchell Greenberg; Almantas Pivrikas ; Ian Gentle ; Bronson Philippa

Appl. Phys. Lett. 127, 112109 (2025)
https://doi.org/10.1063/5.0276562

Applied Physics Letters ARTICLE pubs.aip.org/aip/apl

Charge transport and electric field-dependent exciton dissociation in organic semiconductors measured using accumulation at an insulator–semiconductor layer

Cite as: Appl. Phys. Lett. **127**, 112109 (2025); doi: 10.1063/5.0276562
Submitted: 18 April 2025 · Accepted: 2 September 2025 ·
Published Online: 19 September 2025

Asad Mahmood,[1] Mile Gao,[2] Mitchell Greenberg,[1] Almantas Pivrikas,[3] Ian Gentle,[2] and Bronson Philippa[1,a)]

AFFILIATIONS

[1]College of Science and Engineering, James Cook University, Townsville, Queensland 4814, Australia
[2]Centre for Organic Photonics & Electronics (COPE), School of Chemistry and Molecular Biosciences, The University of Queensland, Brisbane, Queensland 4072, Australia
[3]Physics Department, Murdoch University, Perth, Western Australia 6150, Australia

[a)]**Author to whom correspondence should be addressed:** bronson.philippa@jcu.edu.au

ABSTRACT

Knowledge of charge transport and exciton behavior in organic semiconductor materials is essential to develop high-performance devices. Experimental methods based on the photogeneration of charges offer the opportunity to probe both exciton dissociation and the subsequent charge transport in the same device under the same conditions. In this work, we study the common organic light-emitting diode material tris(2-phenylpyridine)iridium(III), $Ir(ppy)_3$, and show that the yield of free charge carriers from photogenerated excitons is strongly dependent on the electric field in the semiconductor. We simultaneously measure the hole mobility in this material. Our experiments are based on the accumulation of charge carriers at a semiconductor–insulator interface, and we find that the dynamics of this charging process provide information about exciton dissociation and charge carrier mobility. This work illustrates the importance of considering the electric field dependence of exciton dissociation when interpreting charge transport experiments.

The effective transport of charges is essential to the performance of optoelectronic devices such as organic light-emitting diodes (OLEDs).[1] However, charge carrier mobility can be challenging to accurately measure in organic semiconductor thin films due to the confounding influences of the typically disordered morphology,[2–4] the presence of charge traps,[5,6] and the sensitivity of mobility to experimental conditions, including electric field strength[7] and charge carrier concentration.[8] Consequently, a wide variety of techniques have been developed to measure mobility in different situations.[9–11] Of these, experiments based on a metal–insulator–semiconductor (MIS) device structure have emerged as powerful tools for the study of mobility[12–14] and free carrier generation efficiency.[15] In these experiments, a specialized device is constructed with an electrode/insulator/semiconductor/electrode structure. An applied voltage accumulates a specific charge carrier at the insulator–semiconductor interface, either through photogeneration or electrical injection. Charge extraction is performed using linearly increasing voltage (CELIV), which generates a current transient that reveals information about charge transport. The MIS structure's key advantage is its ability to selectively accumulate either electrons or holes based on the applied polarity, allowing for the isolated study of the targeted charge carrier without interference from the other type.

Although MIS-CELIV is a powerful experiment, several challenges remain. If the charges are electrically injected, then there must be a good Ohmic contact between the electrode and semiconductor. However, reliably obtaining an Ohmic contact, especially for electrons, is not always straightforward and may require the time-consuming tuning of fabrication conditions or additional fabrication steps.[16] The injection voltage, injection time, extraction pulse duration, extraction pulse voltage maximum, and the circuit's *RC* time constant all affect

the shape of the transient and must be taken into account when calculating the mobility.[17] While photo-induced MIS-CELIV enables determination of both mobility and free charge carrier generation efficiency without requiring charge injection, the sensitivity to low carrier densities and dependence on optical excitation can pose challenges, particularly in materials with low absorption coefficients or non-uniform film morphology. Most research on MIS-CELIV has concentrated on the charge extraction process, with less focus on the initial charge accumulation at the insulator–semiconductor interface. This phase, often viewed as merely preparatory, involves charge transport (through electrical injection) or the semiconductor bulk (via photogeneration), making it dependent on mobility and other factors. We recently proposed an experiment applying a triangle wave voltage during charge accumulation instead of charge extraction.[18] We now refer to this method as charge *accumulation* by linearly increasing voltage (CALIV) or MIS-CALIV.

A further effect that has not been widely explored but is important for experiments based on linearly increasing voltages is the influence of the electric field dependence of key material properties. Since the electric field is linearly varying during the experiment, any field dependence, especially exciton dissociation yield, confounds the interpretation of the experimental transient. In this paper, we will investigate the field dependence of exciton dissociation yield in the archetypical OLED emissive material tris(2-phenylpyridine)iridium(III), $Ir(ppy)_3$, and measure the hole mobility of the photogenerated charge carriers during this charge accumulation phase at the interface.

The device structure used in our experiments is depicted in Fig. 1(a). This configuration comprises an SiO_2 layer (sputter-coated using AJA ATC 2200 system) serving as the insulator and an $Ir(ppy)_3$ layer (thermally evaporated under high vacuum $<1 \times 10^{-6}$ mbar) acting as the organic semiconductor, each with a thickness of 50 nm. These layers were sandwiched between a transparent metal electrode (ITO, 100 nm) and an aluminum electrode (thermally evaporated under high vacuum $< 1 \times 10^{-6}$ mbar, 100 nm). A function generator (Tektronix 3052C) was employed to apply the voltage across the device, with an oscilloscope (Keysight DSOX3024A) used to record the transients. An LED (part number: 1214-SST-10-SB-B130-M470CT-ND, DigiKey Electronics) with a peak emission wavelength of 470 nm was utilized to produce photo-excited charge carriers. The LED light pulse duration matched the duration of the triangle voltage, i.e., the light was applied throughout the accumulation step.

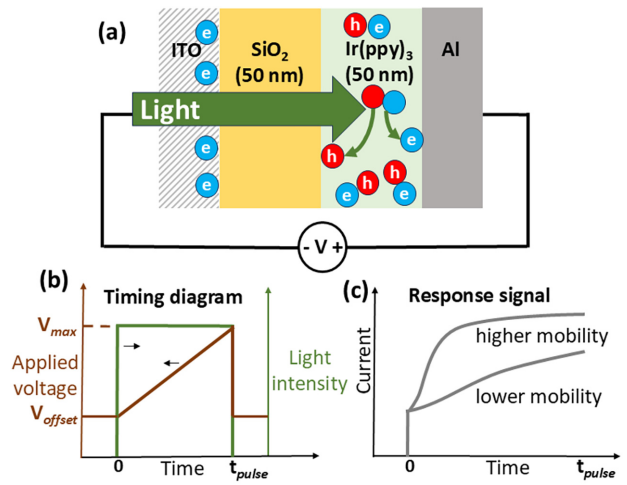

FIG. 1. (a) The device geometry utilized for the MIS-CALIV experiment. (b) The timing diagram includes a triangular voltage pulse (left axis) and a light pulse (right axis). The arrows indicate the axis for each curve. (c) The expected current signals in the cases of high and low mobility. The measured current reaches saturation faster when the mobility is higher, which will be further discussed in the main text.

In our setup, the LED pulse is triggered directly by the same function generator that defines the voltage ramp, ensuring a fixed and reproducible delay with sub-microsecond precision. The LED rise time was measured to be ~0.5 μs using a photodiode, which is negligible relative to the 100 μs voltage ramp. The intensity of the LED was calibrated using a Newport optical power meter (model 1918-C). An illumination area of 2.54 mm^2 was defined using a 3D-printed shadow mask and a condenser lens was used to focus the LED light. While this work focuses primarily on mobility and charge dissociation under different electric fields rather than absolute quantum efficiency, the calibrated intensity ensures that the photogeneration rate is consistent across measurements and sufficient for reliable analysis.

Offset voltages of 5, 10, and 15 V were applied to create varying electric field strengths for exciton separation. A triangular voltage profile with maximum of 20 V was used, as shown in Fig. 1(b). This ramp allowed holes to accumulate near the semiconductor–insulator interface. The current transient response was recorded to study charge carrier properties, with Fig. 1(c) displaying responses for varying mobilities.

This experiment can be understood as the displacement current transitioning between two capacitive charging regimes.[18] Applying a voltage ramp to a capacitor causes a constant charging current given by $I = C\frac{dV}{dt} = CA$, where C is the capacitance and $\frac{dV}{dt} = A$ is the slope of the voltage pulse. The first charging regime begins at the start of the voltage ramp when the device has few charge carriers, and the thickness and dielectric constants of the insulator and semiconductor determine the initial capacitance. The second regime occurs when enough charge accumulates at the semiconductor–insulator interface, leading to a higher capacitance and larger charging current. The transition between these regimes depends on the semiconductor's ability to transport charge, influenced by mobility and exciton dissociation rate under an electric field, which can provide insights into charge transport.

Since an analytic formula to extract the mobility from a MIS-CALIV transient is not available, we used the drift-diffusion model to simulate the transients and fit them to experimental data. The drift-diffusion model is recognized as one of the most dependable and widely adopted approaches for examining the electrical properties of organic semiconductor devices.[19–23] The simulation considers the photoexcitation of excitons (which we approximate as uniform across the semiconductor), the separation of excitons into free charge carriers, and the transport and recombination of those charge carriers. The drift-diffusion solution incorporates the transport of both electrons and holes, even though the purpose of the experiment is to extract the mobility of a single charge carrier. The detailed equations are described in the literature.[19,24–26] The model is based on coupled continuity equations for charge carriers and excitons. Solving these equations involves approximating the partial differential operators.[19,25] We used the finite volume method with 200 numerical grid points to solve the system of equations and obtain the current transient response of

charge carriers. Boundary conditions specified no electron or hole flux at the insulator/semiconductor interface (current density $j = 0$ at this edge). At the semiconductor/electrode interface, holes were permitted to be extracted with the flux calculated by electric field induced drift, while the injection flux for holes was set to zero. Numerical time stepping was implemented by Matlab's ode15s solver.

We assume a constant mobility to simplify the model and reduce the number of free parameters. To keep the modeling results general, we consider variations in the transit time of charge carriers relative to the voltage pulse duration. The transit time is defined as the time taken for a charge carrier to cross the full thickness of the semiconductor layer under the influence of a linearly increasing electric field. By utilizing the fundamental relationship between velocity, electric field, and the distance traveled by charge carriers, we established a relation for the transit time for accumulating charge carriers, which is also included in the literature,[27] given by

$$t_{tr} = \sqrt{\frac{2d_s\left(\frac{\epsilon_s}{\epsilon_i}d_i + d_s\right)}{\mu A}}, \tag{1}$$

where d_s is the semiconductor thickness, d_i is the thickness of the insulator, μ is the mobility of the carriers, A is the slope of the applied voltage (in volts/second), and ϵ_s and ϵ_i are the permittivities of the semiconductor and insulator, respectively. This expression for t_{tr} is defined for the case of zero offset voltage and assumes no charge trapping.

In our curve fitting of the experimental data, we found that considering the electric field's impact on exciton splitting into free charge carriers is crucial. The material Ir(ppy)$_3$, an OLED emitter, does not easily generate free charge carriers upon photogeneration. Generally, organic semiconductors have tightly bound excitons due to a low dielectric constant and strong Coulomb attraction between electron–hole pairs. Exciton separation into free charge carriers is influenced by the electric field and thermal energy. The Onsager–Braun model elucidates how thermal energy and an external electric field contribute to overcoming this Coulomb barrier.[28]

In this work, we have not distinguished between singlet and triplet excitonic states because, in phosphorescent materials like Ir(ppy)$_3$, intersystem crossing from singlet to triplet occurs very rapidly within picoseconds owing to strong spin–orbit coupling. Consequently, most singlet excitons convert to triplets almost immediately. This ultrafast conversion renders the contribution from singlet excitons negligible in our device configuration and timescale. Thus, for modeling charge generation and separation, we consider triplet excitons as the excitons that dissociate into free charge carriers (electrons and holes) under an electric field.

According to the Onsager–Braun model, the probability of exciton dissociation increases with the strength of the applied electric field. The field effectively reduces the energy barrier for separation by distorting the Coulomb potential, thereby facilitating the escape of the electron and hole from their bound state. This model also explains the interplay between exciton dissociation and recombination. The efficiency of separation is determined by the relative changes in these two processes, which depend on the electric field and the properties of the material. In a low electric field regime, the recombination process prevails, leading to a decrease in exciton separation efficiency, which benefits OLED materials. Conversely, in a high electric field scenario, the generation of free charge carriers increases, resulting in more charges being available for the MIS-CALIV experiment.

We applied a simple kinetic model for excitons, incorporating a photogeneration rate X_{gen}, a decay rate, and an electric field-dependent rate of separation into free charge carriers.[29] This results in the following continuity equation for exciton concentration X:[30]

$$\frac{dX}{dt} = X_{gen} - k_{decay}X - k_{sep}(E_{field})X, \tag{2}$$

where k_{decay} denotes the radiative and non-radiative decay constant of excitons, whose value is given by the reciprocal of the exciton lifetime, and k_{sep} gives the charge carriers' separation rate as a function of the applied electric field E_{field}. To keep the numerical model simple, we do not differentiate between singlet and triplet excitons, since we anticipate rapid intersystem crossing in this material. The carriers' separation rate k_{sep} can be empirically approximated by the Onsager–Braun model,[31]

$$k_{sep}(E_{field}) = \frac{3\beta}{4\pi R_s^3}\exp\left(-\frac{E_B}{k_BT}\right)\frac{J_1\left(2\sqrt{-2B}\right)}{\sqrt{-2B}}. \tag{3}$$

Here, the parameter $\beta = \frac{2q\mu}{\epsilon_0\epsilon_s}$ is the Langevin recombination factor with μ as equal mobility of holes and electrons, whereas q is the elementary charge, ϵ_0 is the permittivity of free space, and ϵ_s is the relative permittivity of the semiconductor. The thermal energy is given by k_BT. The Coulomb capture radius is given by $R_s = \frac{q^2}{4\pi\epsilon_s\epsilon_0 k_B T}$.[32,33] The exponential term contains $E_B = \frac{q^2}{4\pi\epsilon_0\epsilon_s R_s}$, which is known as the Coulomb binding energy.[28,34] Using these relations for R_s and E_B, we calculated the numerical values, which are given in Table I. In this expression, J_1 is the Bessel function of the first order having $B = \frac{q^3E_{field}}{8\pi\epsilon_0\epsilon_s k_B^2T^2}$. In our analysis, we are primarily concerned with the yield of free charge carriers, which will depend upon the competition between k_{sep} and k_{decay}. We treat the yield of free carriers at zero field as a fitting parameter, then use the electric field dependence in Eq. (3) to scale the yield at increasing electric field strengths. The electric field dependence is the last

TABLE I. The table details the input parameters employed in the simulation, including material properties, rate constants, and environmental conditions. These values have been strategically chosen to benchmark the simulation results against the experimental data. Some constants and coefficients have been normalized for consistency.

Properties	Values	Source
Relative permittivity of Ir(ppy)$_3$	3.5	Ref. 32
Relative permittivity of SiO_2	3.9	Ref. 37
Yield ($E_{field} = 0$)	4.7%	Fitted
Coulomb capture radius (R_s)	1.58 nm	Calculated
Binding energy (E_B)	274 meV	Calculated
Temperature (T)	300 K	
Resistance $\left(\frac{RC}{t_{pulse}}\right)$	0.016	Fitted
Bimolecular recombination coefficient $\left(\frac{\beta}{\beta_L}\right)$	1	Assumed

factor $\frac{J_1(2\sqrt{-2B})}{\sqrt{-2B}}$. The prefactors are independent of the electric field, which is regarded as a constant term with respect to the electric field.

The differential equation (2) provides an illustration of the dynamics of excitons in organic semiconductors. There are other factors that influence the charge separation rate in organic semiconductors, which can be found in the literature.[32–36] In this study, we are mainly interested in the field dependence and timescale as the main factors influencing the charge transport measurement. Therefore, without going into further details, we focus on the charge separation rate as a function of electric field; the separation yield percentage can be calculated by

$$Yield\% = \left(\frac{k_{sep}(E_{field})}{k_{sep}(E_{field}) + k_{decay}}\right) \times 100. \quad (4)$$

The detailed analysis of the charge separation rate with varying electric fields will be provided later.

We first simulated the ideal case of 100% yield of free charge carriers (both electrons and holes), a situation that is relevant for materials

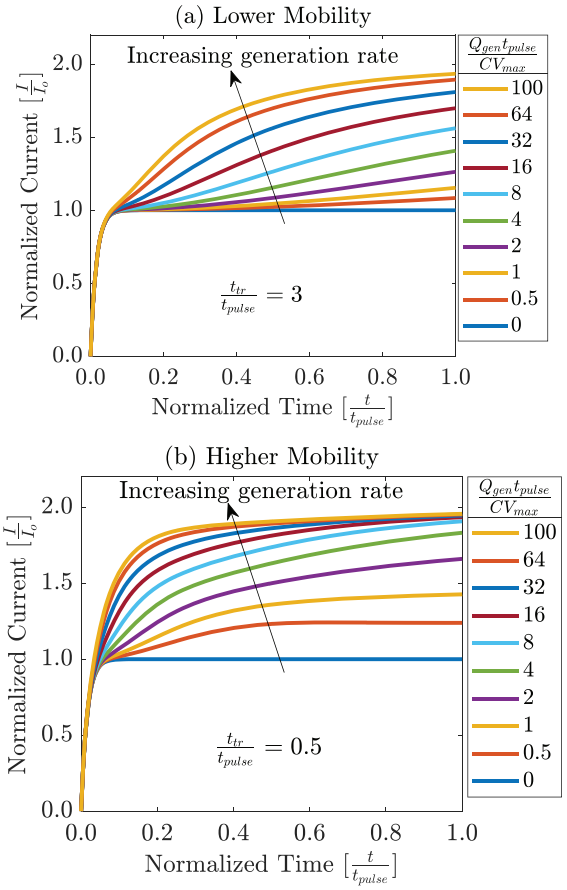

FIG. 2. Illustration of the current transient response across a range of normalized light intensities. Light intensities are represented as the resultant charge carrier generation rate $Q_{gen}t_{pulse}/CV_{max}$.(a) The transient response in the case of $\frac{t_{tr}}{t_{pulse}} = 3$, which implies a relatively low mobility, while (b) depicts the transient response with $\frac{t_{tr}}{t_{pulse}} = 0.5$, which corresponds to a mobility that is 36 times higher than (a).

that can spontaneously split excitons into free charge carriers. Figure 2 shows the results of drift-diffusion simulations, illustrating the normalized current response at various light intensities and charge carrier mobilities. Key parameters included a normalized material recombination coefficient of 1, a resistance of 0.016, and a temperature of 300 K, with equal thicknesses for the semiconductor and insulator. The relative permittivity values were 3.5 for the semiconductor and 3.9 for the insulator. The setup examines how different mobilities affect current behavior in response to a light pulse, with the normalized time axis aiding in generalizing observations for varying pulse durations.

In the lower mobility scenario depicted in Fig. 2(a), the current increases gradually over time due to slower charge carrier transport, resulting in a prolonged period before stabilizing at a steady-state value. As the free charge carrier generation rate rises, the maximum current increases, leading to a flatter curve. This suggests that the accumulation process is slow, with accelerated recombination at higher light intensities to prevent excessive carrier buildup. Consequently, the time to reach maximum current is lengthened at lower light intensities since fewer carriers are generated.

In contrast, Fig. 2(b) shows that with increased mobility, the current reaches its maximum much more rapidly, even at lower light intensities. The sharp increase in current indicates faster carrier transport, allowing for a faster response to light intensity changes. The current accumulates swiftly, causing the curve to flatten earlier than in the lower mobility case. This demonstrates that higher mobility not only accelerates charge accumulation but also influences recombination rates, showcasing the material's effectiveness in transporting and collecting photogenerated carriers.

In curve fitting to the experimental data, we considered field-dependent exciton dissociation, as the electric field strength increases during the voltage pulse. Note that we neglected any field dependence in the mobility as an approximation to simplify the curve-fitting process by reducing the number of free parameters. The field dependence in the exciton dissociation leads to a rising yield of free charge carriers during the voltage ramp. Using the parameters from Table I, Fig. 3 demonstrates exciton separation yield in response to the electric field. The applied offset voltage varies from 5, 10, and 15 V to a maximum triangular voltage of 20 V. At lower offset voltages, the initial yield of free charge carriers is low, while higher voltages generate more carriers throughout the pulse, resembling the ideal case in Fig. 2. Figure 3(b) shows the separation yield over time (microseconds) for different offset voltages, and the inset in Fig. 3(c) illustrates the linear voltage ramp from various offsets to 20 V against time.

At lower electric fields, a slight separation occurs as the electric field strength is too weak to overcome the Coulomb binding energy. However, higher voltages create stronger fields that lower exciton binding energy and increase carrier dissociation probability. The rate of separation rises significantly between low and high field strengths, reaching saturation at high levels. This demonstrates an exponential increase in exciton separation probability with stronger electric fields, due to a reduced potential barrier for charge separation.

Figure 3(b) shows that the separation process starts slowly (under 20 μs) but accelerates between 20 and 40 μs. With increased voltage, almost all excitons become free charge carriers, achieving a maximum separation yield. This is expected, as a stronger electric field weakens electron–hole binding, facilitating their separation.

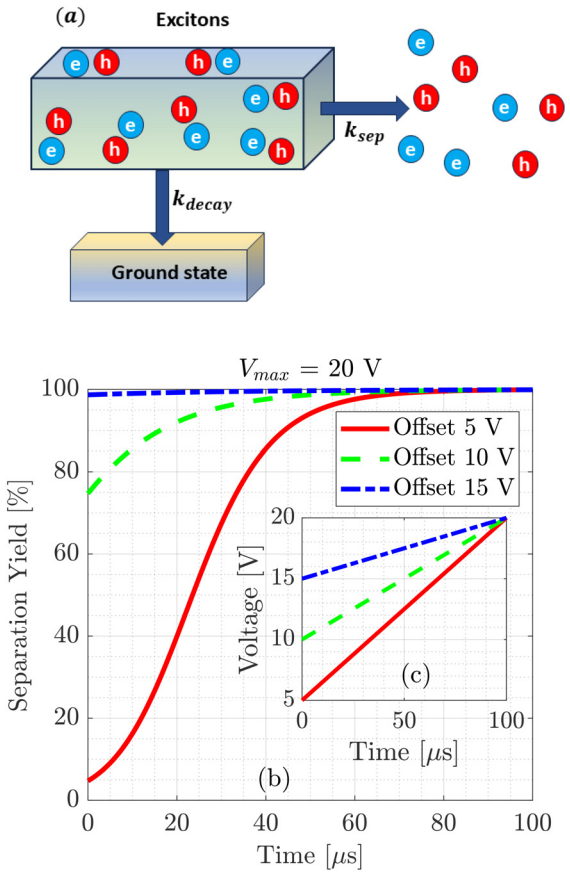

FIG. 3. (a) Illustrates the exciton dynamics within the semiconductor layer, depicting a portion of the exciton decay (k_{decay}) into the ground state while others separate (k_{sep}) into free charge carriers (electrons and holes). (b) Since the applied voltage is linearly increasing, the separation yield of excitons into free charge carriers rises throughout the experiment. (c) The inset shows the applied voltage for each case.

Figure 4 illustrates the experimental data obtained using the MIS-CALIV setup, which was subsequently compared with simulation data derived from the drift-diffusion model. The experimental data were obtained by applying various sets of triangular voltage pulses while maintaining a fixed maximum voltage of $V_{\max} = 20$ V. For reference, the results corresponding to $V_{\max} = 15$ V are included in the supplementary material. During the curve-fitting process, a consistent set of parameters was employed, as detailed in Table I.

The graphs in Fig. 4 illustrate the transient current response as influenced by offset voltage and light intensity under both experimental and simulated conditions. The close alignment between the measured results (noisy lines) and the simulated data (solid lines) confirms the reliability of the drift-diffusion simulation model. The LED power, $P = 0.22$, 0.6, and 1.2 mW, is varied to achieve the exciton generation rate $X'_{gen} = X_{gen} t_{pulse}/CV_{\max} = 0.45$, 1.2, and 2, respectively. In this model, these excitons subsequently separate into free electrons and holes with a yield that depends upon the strength of the electric field.

Moreover, the fitted hole mobility in neat $Ir(ppy)_3$ is $\mu = 1.94 \times 10^{-5} \frac{cm^2}{Vs}$ at a specific condition, which aligns well with the mobility value reported in the literature.[38–40] The key contribution of

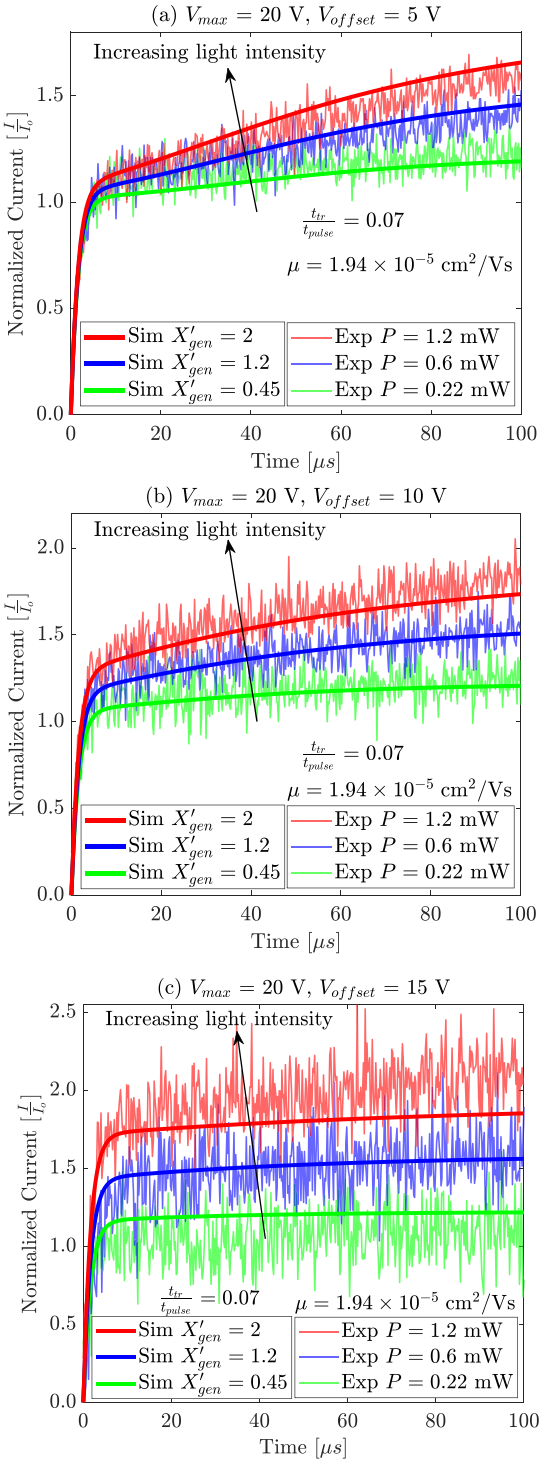

FIG. 4. In this figure, simulated transient plots (sharp color) with continuous exciton generation $X'_{gen} = X_{ge} t_{pulse}/CV_{\max}$ are fitted against experimental results having light intensity with power P. (a), (b), and (c) show the transient response for different offset voltages V_{offset} along with the maximum value of the applied triangular voltage $V_{\max}$.

this result is to demonstrate a method to account for the electric field dependence in the exciton dissociation, an important consideration for CELIV-like experiments. Another point of difference is that using MIS-CALIV, we measure the mobility immediately after the charge generation; on the other hand, in MIS-CELIV, after a long time, which increases the chance of charge trapping and its subsequent impacts. Ultimately, we believe that MIS-CALIV and MIS-CELIV are complementary methods. We intend to explore their simultaneous use in future work.

Figure 4(a) illustrates the transient current response at an offset voltage of $V_{offset} = 5$ V, where a relatively weak electric field is established. Initially, the current density remains low because most of the generated excitons do not dissociate; they begin to do so only as the voltage continues to increase. Over time, the transient current rises as an increasing number of excitons dissociate, generating more free charge carriers. This behavior aligns with the Onsager–Braun model, which indicates that the separation of excitons into free charge carriers is heavily influenced by the strength of the applied electric field.[41,42]

As illustrated in Figs. 4(b) and 4(c), the transient current response exhibits a faster pace at higher offset voltages $V_{offset} = 10$ and 15 V. This increase in offset voltage results in a more intense electric field, which enhances the separation of excitons by diminishing the Coulomb binding energy between electron–hole pairs. Consequently, the slope of the current transient rises more steeply at earlier times, indicating that a more significant portion of the excitons is quickly dissociated into free charge carriers. This characteristic is particularly advantageous for organic solar cells, where efficient charge separation and extraction are vital for achieving high power conversion efficiency.[43] Conversely, in OLEDs, excessive charge separation can be detrimental, as it reduces the availability of excitons for radiative recombination, ultimately leading to efficiency roll-off in the devices.[44]

This study highlights the crucial role of explicitly considering the electric field dependence of exciton dissociation in organic semiconductors. While $Ir(ppy)_3$ is not typically expected to generate free charge carriers effectively under photogeneration due to its tightly bound excitons, our analysis of the insulator–semiconductor interface charging and curve-fitting process reveals that a linearly increasing electric field significantly enhances exciton separation, in alignment with the Onsager–Braun model. As the electric field strength increases, the Coulomb barrier diminishes, leading to a higher probability of dissociation and an increase in transient current. This field-dependent behavior becomes particularly pronounced at elevated offset voltages, where exciton separation occurs more rapidly and efficiently. These findings emphasize the necessity of accounting for field-assisted exciton separation when measuring charge transport properties. We anticipate that the MIS-CALIV technique will offer opportunities to study the combination of exciton separation and charge transport in a variety of organic semiconductor systems.

See the supplementary material for the results corresponding to the case $V_{max} = 15$ V. This includes Figs. 4(d) and 4(e), in which simulated transient plots (sharp color) with continuous exciton generation $X'_{gen} = X_{gen} t_{pulse}/CV_{max}$ are fitted against experimental results having light intensity with power P, showing the transient response for offset voltages $V_{offset} = 5$ and 10 V.

The authors thank Paul L. Burn for helpful discussions. This work was supported by the Australian Research Council Discovery Program (DP210102192).

AUTHOR DECLARATIONS

Conflict of Interest

The authors have no conflicts to disclose.

Author Contributions

Asad Mahmood: Conceptualization (lead); Formal analysis (lead); Investigation (lead); Methodology (equal); Software (equal); Validation (equal); Writing – original draft (lead); Writing – review & editing (equal). **Mile Gao:** Data curation (equal); Formal analysis (equal); Resources (lead); Validation (lead); Visualization (equal); Writing – review & editing (equal). **Mitchell Greenberg:** Formal analysis (equal); Investigation (equal); Software (equal); Writing – review & editing (equal). **Almantas Pivrikas:** Data curation (equal); Formal analysis (equal); Methodology (lead); Validation (lead); Writing – review & editing (equal). **Ian Gentle:** Funding acquisition (equal); Project administration (lead); Writing – review & editing (equal). **Bronson Philippa:** Funding acquisition (lead); Project administration (lead); Resources (lead); Supervision (lead); Validation (lead); Writing – review & editing (equal).

DATA AVAILABILITY

The data that support the findings of this study are available within the article and its supplementary material.

REFERENCES

[1] H. Bässler and A. Köhler, "Charge transport in organic semiconductors," in *Unimolecular and Supramolecular Electronics I* (Springer, Berlin Heidelberg, 2011).
[2] M. Ellis, H. Yang, S. Giannini, O. G. Ziogos, and J. Blumberger, "Impact of nanoscale morphology on charge carrier delocalization and mobility in an organic semiconductor," Adv. Mater. **33**(45), 2104852 (2021).
[3] S. Sanderson, G. Vamvounis, A. E. Mark, P. L. Burn, R. D. White, and B. W. Philippa, "Understanding the performance differences between solution and vacuum deposited OLEDs: A computational approach," J. Chem. Phys. **156**(21), 214703 (2022).
[4] L. Packman, B. Philippa, A. Pivrikas, P. L. Burn, and I. R. Gentle, "Reconstructing the 3D coordinates of guest:host OLED blends with single atom resolution," Small Methods **8**, 2301305 (2024).
[5] H. F. Haneef, A. M. Zeidell, and O. D. Jurchescu, "Charge carrier traps in organic semiconductors: A review on the underlying physics and impact on electronic devices," J. Mater. Chem. C **8**(3), 759–787 (2020).
[6] S. Sanderson, B. Philippa, G. Vamvounis, P. L. Burn, and R. D. White, "Elucidating the effects of guest-host energy level alignment on charge transport in phosphorescent OLEDs," Appl. Phys. Lett. **115**(26), 263301 (2019).
[7] M. Bouhassoune, S. L. M. van Mensfoort, P. A. Bobbert, and R. Coehoorn, "Carrier-density and field-dependent charge-carrier mobility in organic semiconductors with correlated Gaussian disorder," Org. Electron. **10**(3), 437–445 (2009).
[8] S. Sanderson, B. Philippa, G. Vamvounis, P. L. Burn, and R. D. White, "Understanding charge transport in $Ir(ppy)_3$:CBP OLED films," J. Chem. Phys. **150**(9), 094110 (2019).
[9] S. Tiwari and N. C. Greenham, "Charge mobility measurement techniques in organic semiconductors," Opt. Quantum Electron. **41**(2), 69–89 (2009).
[10] A. J. Mozer, N. S. Sariciftci, L. Lutsen, D. Vanderzande, R. Österbacka, M. Westerling, and G. Juška, "Charge transport and recombination in bulk heterojunction solar cells studied by the photoinduced charge extraction in linearly increasing voltage technique," Appl. Phys. Lett. **86**(11), 112104 (2005).
[11] M. Neukom, S. Züfle, S. Jenatsch, and B. Ruhstaller, "Opto-electronic characterization of third-generation solar cells," Sci. Technol. Adv. Mater. **19**(1), 291–316 (2018).

[12]S. Dahlström, X. Liu, Y. Yan, O. J. Sandberg, M. Nyman, Z. Liang, and R. Österbacka, "Extraction current transients for selective charge-carrier mobility determination in non-fullerene and ternary bulk heterojunction organic solar cells," ACS Appl. Energy Mater. **3**(9), 9190–9197 (2020).
[13]J. Peng, X. Chen, Y. Chen, O. J. Sandberg, R. Österbacka, and Z. Liang, "Transient extraction of holes and electrons separately unveils the transport dynamics in organic photovoltaics," Adv. Electron. Mater. **2**(3), 1500333 (2016).
[14]S. Züfle, S. Altazin, A. Hofmann, L. Jäger, M. T. Neukom, T. D. Schmidt, W. Brütting, and B. Ruhstaller, "The use of charge extraction by linearly increasing voltage in polar organic light-emitting diodes," J. Appl. Phys. **121**(17), 175501 (2017).
[15]M. Gao, S. McAnally, H. Jin, P. L. Burn, A. Pivrikas, and P. E. Shaw, "Free carrier generation efficiency in organic photovoltaic films determined using photo-MIS-CELIV," Org. Electron. **135**, 107137 (2024).
[16]D. Trieb, P. W. M. Blom, and G.-J. Wetzelaer, "Ohmic electron injection into organic semiconductors by solution-processed and evaporated organic interlayers," Adv. Mater. Interfaces **10**(19), 2202424 (2023).
[17]M. Gao, P. L. Burn, and A. Pivrikas, "Charge transport in an organic light emitting diode material measured using metal-insulator-semiconductor charge extraction by linearly increasing voltage with parameter variation," J. Appl. Phys. **126**(3), 035501 (2019).
[18]M. Gao, P. L. Burn, G. Juška, and A. Pivrikas, "Unequilibrated charge carrier mobility in organic semiconductors measured using injection metal–insulator–semiconductor charge extraction by linearly increasing voltage," Adv. Photonics Res. **5**, 2300325 (2024).
[19]S. Saggar, A. Mahmood, N. Nayak, A. Kumar, M. R. Andersson, B. Philippa, S.-C. Lo, and E. B. Namdas, "Response speed of organic photodiodes as a function of incident optical intensity," Adv. Opt. Mater. **12**(16), 2302916 (2024).
[20]S. Altazin, C. Kirsch, E. Knapp, A. Stous, and B. Ruhstaller, "Refined drift-diffusion model for the simulation of charge transport across layer interfaces in organic semiconductor devices," J. Appl. Phys. **124**(13), 135501 (2018).
[21]C. Groves, "Simulating charge transport in organic semiconductors and devices: A review," Rep. Prog. Phys. **80**, 026502 (2017).
[22]E. Knapp, R. Häusermann, H. U. Schwarzenbach, and B. Ruhstaller, "Numerical simulation of charge transport in disordered organic semiconductor devices," J. Appl. Phys. **108**(5), 054504 (2010).
[23]M. Darwish and A. Gagliardi, "A drift-diffusion simulation model for organic field effect transistors: On the importance of the Gaussian density of states and traps," J. Phys. D **53**(10), 105102 (2020).
[24]K. Zojer, "Simulation of charge carriers in organic electronic devices: Methods with their fundamentals and applications," Adv. Opt. Mater. **9**(14), 2100219 (2021).
[25]B. Philippa, M. Stolterfoht, P. L. Burn, G. Juška, P. Meredith, R. D. White, and A. Pivrikas, "The impact of hot charge carrier mobility on photocurrent losses in polymer-based solar cells," Sci. Rep. **4**(1), 5695 (2014).
[26]B. Philippa, C. Vijila, R. D. White, P. Sonar, P. L. Burn, P. Meredith, and A. Pivrikas, "Time-independent charge carrier mobility in a model polymer: Fullerene organic solar cell," Org. Electron. **16**, 205–211 (2015).
[27]A. Armin, G. Juska, M. Ullah, M. Velusamy, P. L. Burn, P. Meredith, and A. Pivrikas, "Balanced carrier mobilities: Not a necessary condition for high-efficiency thin organic solar cells as determined by MIS-CELIV," Adv. Energy Mater. **4**(4), 1300954 (2014).
[28]D. Liraz and N. Tessler, "Charge dissociation in organic solar cells—From Onsager and Frenkel to modern models," Chem. Phys. Rev. **3**(3), 031305 (2022).
[29]M. A. Baldo, D. F. O'Brien, M. E. Thompson, and S. R. Forrest, "Excitonic singlet-triplet ratio in a semiconducting organic thin film," Phys. Rev. B **60**(20), 14422–14428 (1999).
[30]D. Kasemann, R. Brückner, H. Fröb, and K. Leo, "Organic light-emitting diodes under high currents explored by transient electroluminescence on the nanosecond scale," Phys. Rev. B **84**(11), 115208 (2011).
[31]J. Kern, S. Schwab, C. Deibel, and V. Dyakonov, "Binding energy of singlet excitons and charge transfer complexes in MDMO-PPV:PCBM solar cells," Phys. Status Solidi (RRL) **5**(10–11), 364–366 (2011).
[32]T. M. Clarke and J. R. Durrant, "Charge photogeneration in organic solar cells," Chem. Rev. **110**(11), 6736–6767 (2010).
[33]K. M. Pelzer and S. B. Darling, "Charge generation in organic photovoltaics: A review of theory and computation," Mol. Syst. Des. Eng. **1**(1), 10–24 (2016).
[34]P. Grygiel, K. Falkowski, D. Pelczarski, and W. Stampor, "Sano-Tachiya-Noolandi-Hong, Onsager and Braun models vs Monte Carlo simulation of charge photogeneration in organic solids," Org. Electron. **39**, 328–339 (2016).
[35]A. Armin, W. Li, O. J. Sandberg, Z. Xiao, L. Ding, J. Nelson, D. Neher, K. Vandewal, S. Shoaee, T. Wang, H. Ade, T. Heumüller, C. Brabec, and P. Meredith, "A history and perspective of non-fullerene electron acceptors for organic solar cells," Adv. Energy Mater. **11**(15), 2003570 (2021).
[36]X. de Vries and R. Coehoorn, "Vibrational mode contribution to the dielectric permittivity of disordered small-molecule organic semiconductors," Phys. Rev. Mater. **4**(8), 085602 (2020).
[37]P. Zukowski, T. N. Koltunowicz, K. Czarnacka, A. K. Fedotov, and I. E. Tyschenko, "Carrier transport and dielectric permittivity of SiO_2 films containing ion-beam synthesized InSb nanocrystals," J. Alloys Compd. **846**, 156482 (2020).
[38]W. Choi, C. Cheung, and S. K. So, "Can an organic phosphorescent dye act as a charge transporter?," Org. Electron. **11**(5), 872–875 (2010).
[39]M. Gao, P. L. Burn, and A. Pivrikas, "Balanced hole and electron transport in Ir(ppy)3:TCTA blends," ACS Photonics **8**(8), 2425–2430 (2021).
[40]M. Gao, T. Lee, P. L. Burn, A. E. Mark, A. Pivrikas, and P. E. Shaw, "Revealing the interplay between charge transport, luminescence efficiency, and morphology in organic light-emitting diode blends," Adv. Funct. Mater. **30**(9), 1907942 (2020).
[41]L. Onsager, "Initial recombination of ions," Phys. Rev. **54**(8), 554–557 (1938).
[42]C. L. Braun, "Electric field assisted dissociation of charge transfer states as a mechanism of photocarrier production," J. Chem. Phys. **80**(9), 4157–4161 (1984).
[43]G. Yu, J. Gao, J. C. Hummelen, F. Wudl, and A. J. Heeger, "Polymer photovoltaic cells: Enhanced efficiencies via a network of internal donor-acceptor heterojunctions," Science **270**(5243), 1789–1791 (1995).
[44]M. A. Baldo, D. F. O'Brien, Y. You, A. Shoustikov, S. Sibley, M. E. Thompson, and S. R. Forrest, "Highly efficient phosphorescent emission from organic electroluminescent devices," in *Electrophosphorescent Materials and Devices* (Jenny Stanford Publishing, 2023), pp. 1–11.